ADVANCED OPTICAL MATERIALS
www.advopticalmat.de

Self-Assembled 2D Sheets of an Amphiphilic Sexiphenyl Exhibit Intense Polarized Blue Emission in the Solid State

Pramita Mondal, Jonathan P. Hill, Gouranga Manna, Sharmistha De Dalui, Edward A. Neal, Gary. J. Richards, Katsuhiko Ariga, Yusuke Yamauchi, Lok Kumar Shrestha, and Somobrata Acharya**

Distinct from inorganic 2D nanomaterials (e.g., graphene, MoS_2, etc,), self-assembled organic 2D materials are significant due to the unique advantages of fine structure tunability and functionality. Electronically and photofunctionally-active compounds (e.g., pentacene, *p*-sexiphenyl) are highly attractive for applications but are limited by difficult handling and the existence of only a few native structures of the compounds. Here, it is shown that a *p*-sexiphenyl derivative incorporated into 2D multilamellar sheets with chromophores oriented in the layers exhibits a significant polarization of photoluminescence. Highly emissive, amphiphilic sexiphenyl with hydrophilic/hydrophobic groups self-assembles at air–water interface with chromophore orientation in the resulting films being controlled by monolayer compression. Large-area multilamellar structures with *p*-sexiphenyl chromophores highly oriented against the 2D plane are prepared by consecutive film transfers. The 2D sheets exhibit significant polarization of photoluminescence with polarization ratio 0.8 between orthogonal in-plane axes. Notably, multilamellar structures cannot be established for the same *p*-sexiphenyl using thermotropic processing thus emphasizing the importance of the 2D sheet multilayer synthesis process. Amphiphile design can be applied for the tailored synthesis of large-area multilayered 2D sheets and used to construct highly efficient light-emitting devices.

1. Introduction

Atomic scale ultrathin 2D nanosheets, such as graphene,[1] hexagonal boron nitride,[2] or MXenes,[3] have drawn significant interest owing to their exceptional electronic, optical, thermal, and mechanical properties with strongly anisotropic features for applications in flexible optoelectronics, catalysis, bioimaging, and energy storage.[4–8] Despite the growing interest in this field, the synthesis of 2D assemblies, especially bulk multilayer or freestanding materials, remains a challenging task. Notwithstanding the molecular phenomenon of aggregation-induced emission (AIE),[9] solid-state organic 2D nanosheets do not usually exhibit intense fluorescence due to self-quenching[10] or aggregation-induced quenching.[11] However, few-layered organic 2D nanosheets exhibiting high photoluminescence (PL) quantum yields offer several advantages in certain organic optoelectronic applications.[3,12] Similarly to the case of inorganic 2D nanosheets, an important criterion to be fulfilled for

P. Mondal, S. De Dalui, S. Acharya
School of Applied and Interdisciplinary Sciences
Indian Association for the Cultivation of Science
Jadavpur, Kolkata, West Bengal 700032, India
E-mail: camsa2@iacs.res.in

J. P. Hill, E. A. Neal, K. Ariga, L. K. Shrestha
Research Center for Materials Nanoarchitectonics
National Institute for Materials Science
Namiki 1-1, Tsukuba, Ibaraki 305-0044, Japan
E-mail: jonathan.hill@nims.go.jp

The ORCID identification number(s) for the author(s) of this article can be found under https://doi.org/10.1002/adom.202400177

DOI: 10.1002/adom.202400177

G. Manna
Surface Physics and Materials Science Division
Saha Institute of Nuclear Physics
1/AF Bidhan Nagar, Kolkata 700064, India

G. J. Richards
Department of Applied Chemistry
Graduate School of Engineering and Science
Shibaura Institute of Technology
Fukasaku 307, Minuma-ku, Saitama-shi, Saitama 337-8570, Japan

K. Ariga
Department of Advanced Materials Science
Graduate School of Frontier Sciences
The University of Tokyo
5-1-5 Kashiwanoha, Kashiwa, Chiba 277-8561, Japan

Y. Yamauchi
Department of Materials Process Engineering, Graduate School of Engineering
Nagoya University
Nagoya 464-8603, Japan

Y. Yamauchi
Department of Chemical and Biomolecular Engineering
Yonsei University
50 Yonsei-ro, Seodaemun-gu, Seoul 03722, South Korea

the applications of organic self-assembled 2D and 3D systems is a high degree of polarization anisotropy in order to establish superior optical switching and display-device performance.[13,14] In particular, long-range orientational order of organic molecules can promote control over the polarization anisotropy. For example, controlling long-range molecular order determines intra-assembly excitation delocalization and relaxation pathways, and is central to the design of artificial light-harvesting systems using synthetic molecular assemblies.[15,16] For π-electronic systems, the molecular orientation of the chromophores is usually perpendicular to the long axis of, for instance, 1D fibers. This is essentially due to spontaneous π-stacking of the molecules usually enforced by van der Waals interactions.[15,17] While molecular orientational control of excited state properties of spontaneously oriented supramolecular π-conjugated systems is a challenging task, the precise tuning of molecular alignment can be achieved in organic 2D sheets using self-assembly at the air–water interface by controlling the surface pressure in Langmuir–Blodgett (L–B) technique, and by applying molecular design principles to affect the orientation of molecules aggregated under interfacial conditions.

The compound *p*-sexiphenyl (1,1′:4′,1′′:4′′,1′′′:4′′′,1′′′′:4′′′′,1′′′′′-sexiphenyl) was first prepared around a century ago and, despite subsequent difficulties with its synthesis and purification,[18] it is regarded as a promising semiconductor and optoelectronic material due to its excellent thermal stability and high PL quantum yield in the solid state.[19,20] Sexiphenyl exhibits a wide bandgap,[21] strong blue PL[22] and large hole mobility,[21–23] and can be obtained in thin film form making it suitable for applications in organic transistors[22] and other optical device architectures. Polarized electroluminescence has been stimulated from an oriented *p*-sexiphenyl film,[24] while full-color applications are also achievable by converting the deep blue light generated by *p*-sexiphenyl into green and red using the proper dye layers and filters.[25,26] Based on the reported properties of its films, its extended linear molecular morphology, which suggests linear polarization activity, and a perceived synthetic flexibility, we have selected *p*-sexiphenyl as a chromophore for the design and assembly as 2D sheets using the LB method.

In this work, we introduce an amphiphilic sexiphenyl derivative **ASP-1** (see **Figure 1**) designed specifically for self-assembly at the air–water interface. Interestingly, the resulting multilayer 2D sheets exhibit intense blue luminescence, an unusual feature for planar chromophores.[27,28] The interfacial self-assembly process of formation of the 2D sheets was monitored using atomic force microscopy (AFM) performed at different stages of the assembly process. The multilayer of the 2D sheets of the sexiphenyl derivatives form a lamellar structure based on the alternation of layering of the amphiphile. Sexiphenyl molecules are strongly aligned within the 2D sheets as a consequence of the deposition process and the extended molecular morphology. This was confirmed by using polarized PL spectroscopy. The 2D sheets exhibit large polarization anisotropy again indicating the strong alignment of **ASP-1** molecules with orientation perpendicular to the long axes of the 2D sheets. Thus, the molecular design concept in combination with the interfacial technique at the water surface can be considered a highly promising method for the design and construction of polarized organic luminescent 2D sheets.[29,30]

2. Results and Discussion

2.1. Synthesis

Sexiphenyl derivative **ASP-1** was synthesized by a mixed Suzuki coupling reaction of two dendronized biphenyl derivatives (3,4,5-tris(n-dodecyloxybenzyl/ (3,4,5-tris(2-(2-(2-methoxyethoxy)ethoxy)ethoxy)benzyl dendrons; see Supporting Information for details) with 4,4′-biphenylboronic acid followed by separation of the three main products using column chromatography, gel permeation chromatography and a final "recrystallization" step from tetrahydrofuran (THF) where **ASP-1** was dissolved in hot THF and a gel monolith allowed to form by cooling at 5 °C. Subsequent decantation of non-gelated THF or cold filtration led to highly pure **ASP-1**, which is amphiphilic based on its hydrophobic/hydrophilic substituents. Importantly, hydrophilic oligoethylene glycol units are essentially dissolved in the water subphase when spread at an air–water interface[31] while the hydrophobic alkoxy-substituted group is repelled away from the water subphase. This provides a strong basis for the assembly of the molecules especially where a lateral force can be applied to manipulate the molecular spacing in situ. The *p*-sexiphenyl unit is also highly hydrophobic and will reside away from the water subphase with inter-chromophore interactions (π–π, C—H…π) promoting the formation of ordered layered structures. Figure 1a shows the chemical structure of **ASP-1** and a graphical representation of the molecule, where the long rigid sexiphenyl chromophore is appended at its opposing extremities with dendron-like substituents (green cone = hydrophilic; red cone = hydrophobic) attached through flexible benzyloxy linkages (indicated by balls). Although coplanarity of the phenyl rings is anticipated based on X-ray crystallographic measurements,[32] the molecules may be non-coplanar since they are known to undergo librational motion in particular when not constrained by a crystal lattice or at an interface. The compound is highly fluorescent in the solution and solid states (Figures 1b,c, resp.), forms a gel in THF (Figures 1d–g), forms self-assembled fibers under precipitation from solution (Figure 1h), and also forms a liquid crystal mesophase at elevated temperature (Figure 1i) the latter being assigned as a lamellar tetragonal structure similar to that observed for other dendron-rod-type molecules.[33]

Y. Yamauchi
Australian Institute for Bioengineering and Nanotechnology (AIBN)
The University of Queensland
Brisbane, QLD 4072, Australia
L. K. Shrestha
Department of Materials Science, Faculty of Pure and Applied Sciences
University of Tsukuba
1-1-1 Tennodai, Tsukuba, Ibaraki 305-8573, Japan
S. Acharya
Technical Research Center (TRC)
Indian Association for the Cultivation of Science
Jadavpur, Kolkata 700032, India

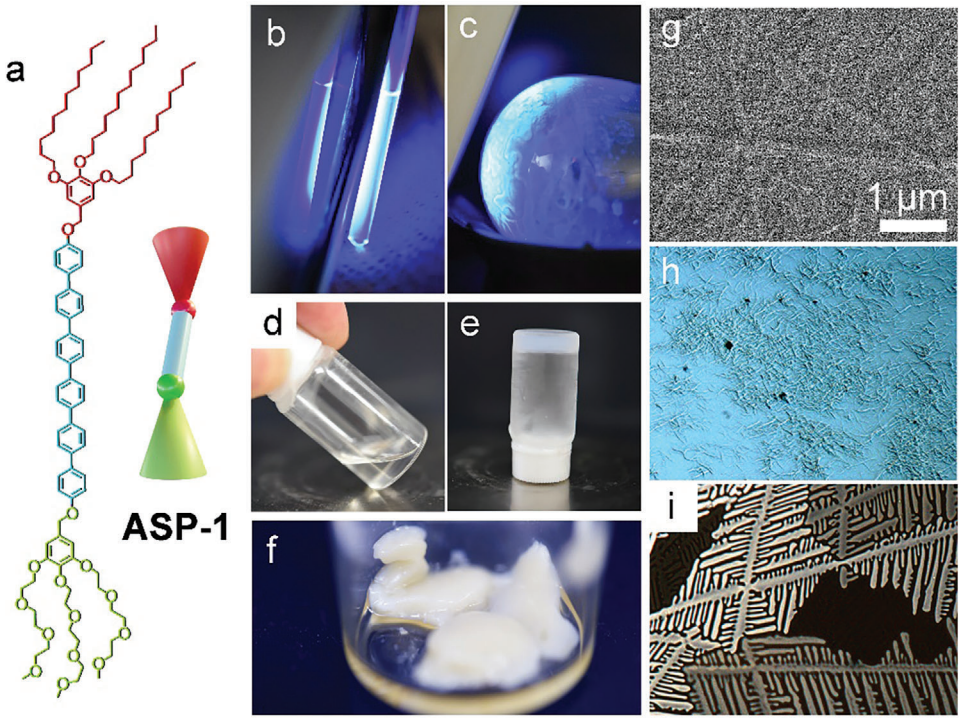

Figure 1. Structure and characteristics of **ASP-1**. a) Chemical structure and graphical representation of the sexiphenyl amphiphile **ASP-1** used in this work. b) Solution of **ASP-1** in $CDCl_3$ (4 mg mL^{-1}) under irradiation using 365 nm ultraviolet light eliciting intense white-blue fluorescence. c) Fluorescence of **ASP-1** in the solid state under irradiation with 365 nm UV lamp. d) Photograph of a solution of **ASP-1** (2 mg mL^{-1} in tetrahydrofuran). e) Photograph of the gel formed on cooling the solution in (d) for 2 h at 5 °C. f) Gel state of **ASP-1** (10 mg mL^{-1} in tetrahydrofuran) formed during purification. g) Scanning electron microscopy (SEM) image of the xerogel formed from the 10 mg mL^{-1} gel state. h) Fibres formed by diffusing methanol into a toluene solution of **ASP-1**. i) Fern-like optical texture (cross polarizers at 90°) of a solid sample of **ASP-1** at 220 °C after cooling from an isotropic melt indicates a tetragonal mesophase structure. (g) Schematic illustrating the limiting molecular area (A = 120 $Å^2$) and its origin. (h) Method for preparation of multi-layered film by repetitive immersion and withdrawal of a mica substrate through the compressed monolayer of **ASP-1** at the air–water interface.

2.2. Monolayer Formation and Structure

The surface pressure (π) versus area/molecule (A) isotherm (Figure S1a, Supporting Information, red curve) shows a phase transition from a 2D liquid-expanded phase at low surface pressure to liquid condensed phase, which collapses at ≈65 mN m^{-1}. A limiting molecular area of ≈120 $Å^2$ per molecule was extracted from the π–A isotherm curve, which is substantially lower than the area expected for a single **ASP-1** molecule calculated using a minimum energy conformation (≈1210 $Å^2$; see also Figure S2, Supporting Information). The calculated area per molecule is similar to those reported for molecules also substituted with hydrophilic dendron-like substituents and is a characteristic of the interaction of such dendrons with the subphase where molecules stand orthogonal to the subphase surface leading to low values of limiting molecular area.[34] We have carried out surface potential measurements of **ASP-1** derivatives at the air–water interface during the uniaxial compression process (Figure S1a, Supporting Information, blue curve). An optimal dipole moment is expected for the parallel arrangement of **ASP-1** derivatives molecules. The surface potential (ΔV) versus area (A) isotherm does not show a change at the initial stage of compression, which is larger than the limiting area per molecule observed in the π–A isotherm curve. The π–A isotherm reflects van der Waals interactions between the hydrocarbon chains and π–π interactions of the **ASP-1** derivatives, while the ΔV–A isotherm is dominated by long-range dipole-dipole interactions.[35] A rapid compression-induced increase of the effective molecular dipole moment is observed at higher surface pressure suggesting a preferred orientation of the **ASP-1** dipole moment perpendicular to the lifting direction of the LB films. We have investigated the film stability by performing successive compression-expansion isotherm cycles below the collapse pressure as shown in Figure S1a (Supporting Information) blue curve.

The dependence of film dimensions and morphology of the self-assembled monolayers of **ASP-1** was observed by lifting the monolayer at different surface pressures selected according to the π-A isotherm. Atomic force microscopy (AFM) images (**Figure 2**) reveal the formation of narrow interconnected fiber-like structures at low surface pressures (5 mN m^{-1}; see Figures 2a,g). With increasing surface pressure, the fibrous structures gradually merge eventually yielding a homogeneous 2D sheet structure at a surface pressure of 35 mN m^{-1} (Figures 2e,k). Figure 2 also shows AFM images of the monolayer lifted at 10 mN m^{-1} (Figure 2b,h), 15 mN m^{-1} (Figure 2c,i), and 25 mN m^{-1} (Figure 2d,j) revealing a progressive shrinking and elimination of void spaces in the monolayer by lateral merging of fibers. Small voids remain in the monolayer film at surface pressure π = 25 mN m^{-1} but these are absent in the uniform film obtained at 35 mN m^{-1} (Figure 2e,k). AFM height profile measurements reveal

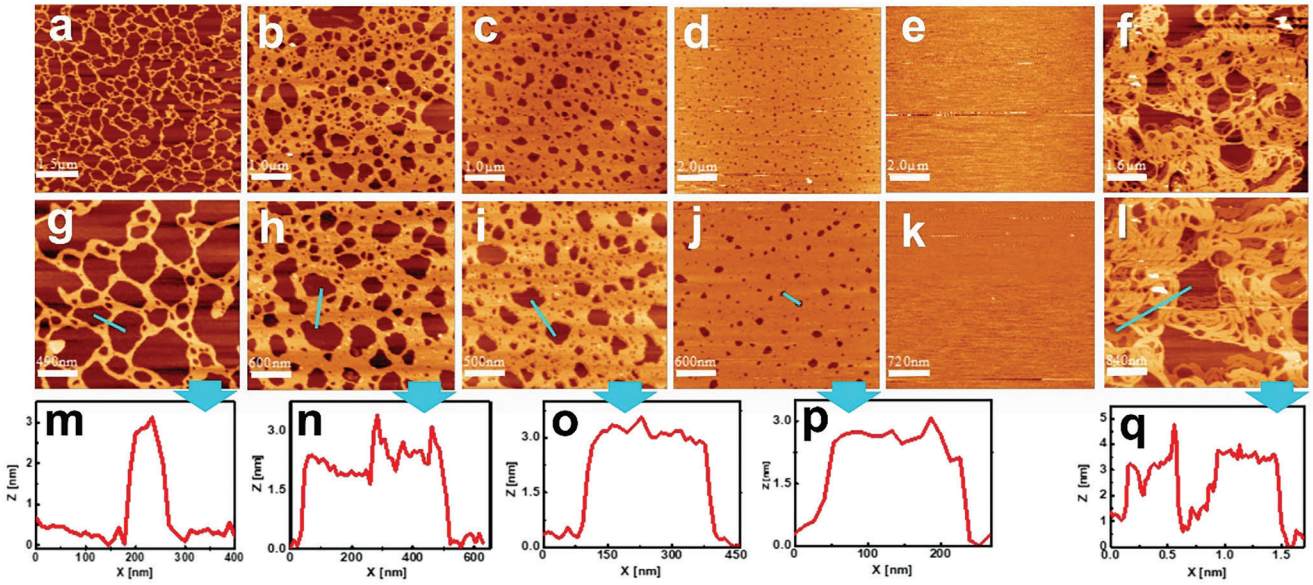

Figure 2. Atomic force microscopy (tapping mode, AFM tip (Si) radius: <10 nm) images of **ASP-1** at different surface pressures. a) 5 mN m^{-1} b) 10 mN m^{-1}, c) 15 mN m^{-1}, d) 25 mN m^{-1}, e) 35 mN m^{-1}, f) dropcast film (10^{-6} M). Corresponding higher magnification AFM images are shown in g) 5 mN m^{-1}, h) 10 mN m^{-1}, i) 15 mN m^{-1}, j) 25 mN m^{-1}, k) 35 mN m^{-1} and l) dropcast films (10^{-6} M). Height profile analyses for AFM images (indicated by blue lines/arrows): m) 5 mN m^{-1}, n) 10 mN m^{-1}, o) 15 mN m^{-1}, p) 25 mN m^{-1} and q) dropcast film (10^{-6} M). Data indicates monolayer height ≈3.5 ± 0.5 nm at all surface pressures (also in the drop-cast film) although measured heights of soft materials are generally underestimated by this method[36] and are also affected by water layer on mica substrate.[37] Films shown in (e) and (k) were smooth with no measurable nanometric features.

a uniform average height of ≈3.5 ± 0.5 nm at all surface pressures (Figures 2m–p). The constant height of the films indicates the consolidation of the fibers into a final 2D sheet of similar thickness. Interestingly, drop-casting of a chloroform solution of **ASP-1** onto mica yields a nanofiber network (Figure 2f,l) similar to that observed at low surface pressures and the gel fibers of **ASP-1** formed in THF (see Figure 1). However, 2D sheet could not be formed by simple drop-casting indicating that processing of **ASP-1** at the air–water interface is important for their synthesis.

2.3. Optical Properties of ASP-1 Sheet

Electronic absorption (UV–vis) spectra of monolayer LB films deposited at various surface pressures and a UV–vis spectrum of **ASP-1** in chloroform solution (10^{-6} M) are shown in **Figure 3**a. In solution, **ASP-1** exhibits a broad peak at 320 nm assigned to the $\pi \rightarrow \pi^*$ electronic transition of the sexiphenyl chromophore. In monolayer films, the corresponding absorption peak is red-shifted by ≈20 nm and a weak additional absorbance appears at 390 nm. These minor changes indicate *J*-type aggregation caused by specific molecular processes at the air–water interface. The absorbance of monolayer films increases as the surface pressure increases without variation of the peak position indicating an increasing density of chromophore molecules per area of the lifted films, and that there is no variation in intermolecular interactions within the monolayers. PL spectra of the same **ASP-1** monolayers and solution are shown in Figure 3b. In solution, the spectrum contains two overlapping peaks at ≈388, 405 nm with a shoulder at ≈432 nm (Figure 3b). The spectra of the monolayer LB films

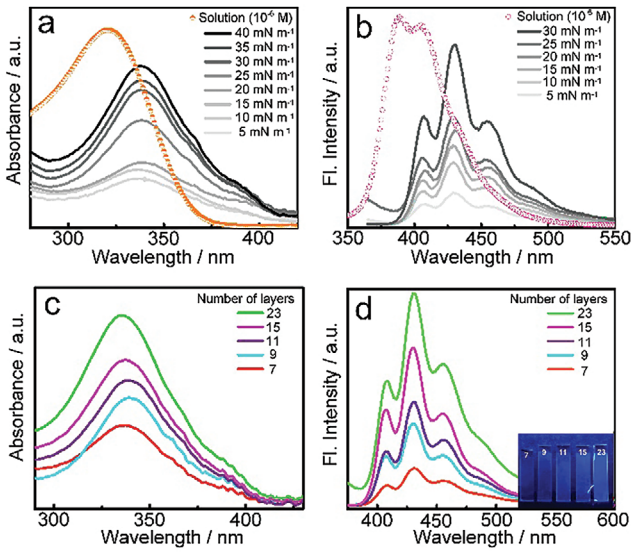

Figure 3. Photophysical properties and structure of **ASP-1** in solution and film states. a) Electronic absorption (UV–vis) spectra of **ASP-1** in chloroform solution (10^{-6} M) and in monolayer **ASP-1** films lifted at the surface pressures shown. The ≈20 nm red shift in λ_{max} LB films suggests aggregation of the chromophores at air–water interface. b) Photoluminescence spectra of **ASP-1** in chloroform solution (10^{-6} M) and monolayer films lifted at the surface pressures shown. c) UV–vis absorption spectra of LB multilayer **ASP-1** films deposited at 25 mN m^{-1}. Layer number is given. d) Photoluminescence spectra of LB multilayer **ASP-1** films with increasing layer number. Inset: photographs of LB films under 365 nm UV illumination. Layer number shown, deposited at 25 mN m^{-1}.

of **ASP-1** contain three better-resolved peaks at 407, 431, and 454 with a shoulder at 490 nm (Figure 3b). PL peaks of the monolayers can be assigned to contributions from vibronic transitions at 3.11 eV (0–0), 2. 93 eV (0–1) (dominant), 2.76 eV (0–2), and a weaker feature around 2.58 eV (0–3).[19,38] UV–vis absorption and PL spectra of the multilayered LB films lifted at 25 mN m^{-1} are shown in Figure 3c,d, respectively. UV–vis absorption spectra of multilayer films contain a broad peak at ≈340 nm (same as for the monolayers), which hardly shifts with increasing layer number. Absorbance of the LB films increases uniformly with increasing layer number due to the increasing thickness of the multilayer film (Figure 3c). PL spectra of multilayer LB films of **ASP-1** contain peaks at 407, 431, 454, and 490 nm with a layer-number-coupled increase in intensity (Figure 3d). A lack of any substantial variation in absorbance and PL peaks indicate that the structure of the films persists in the Langmuir monolayers and upon transfer as multilayer LB films.[39] Multilayer films of 2D sheets deposited on a quartz substrate exhibit strong blue emission under 365 nm UV illumination (see photograph inset of Figure 3d, also Figure 1b,c).

ASP-1 exhibits a PL quantum yield (PLQY) of ≈55% (Table S1, Supporting Information) in solution. PL quantum yields of a monolayer, LB-formed 2D sheets, and drop-cast film are lower probably due to non-radiative dissipation caused by the close π–π approach of the sexiphenyl moieties. LB-formed 2D sheets lifted at different surface pressures of 10 and 25 mN m^{-1} have PL quantum yields of 12.79% and 40.51%, respectively. This enhancement of PL quantum yield with increasing surface pressure indicates that PL is quenched in the small aggregates of ASP-**1** formed at low pressure at the air–water interface but is enhanced at higher surface pressure during 2D sheet formation. Drop-cast film has PL quantum yield (16.1%) similar to that of a monolayer film deposited at 10 mN m^{-1}, which is not surprising based on their similar coverages and morphologies (see Figure 2). Fluorescence microscopy of a 3-layer film lifted at a surface pressure of 25 mN m^{-1} (Figure S3, Supporting Information) indicates increasing optical response with increasing layer number as is also obvious from the PL emission from multilayer films shown in the inset of Figure 3d.

2.4. Structure of Multilayer ASP-1 Sheet

Bulk orientation of chromophores contained in self-assembled structures is an important parameter in any potential applications of organic self-assembled materials.[40,41] This aspect has been probed here for **ASP-1** using linear dichroism (LD) spectroscopy on films obtained during the fibers to 2D sheet transformation to monitor the intrinsic dipole moment alignment in the molecular assembly. The LD spectrum of **ASP-1** film (**Figure** 4a) contains an intense negative peak at 337 nm with a weaker negative shoulder (associated with *J*-type aggregation) at 389 nm. The negative LD signal indicates a greater perpendicular (A⊥) than parallel (A∥) absorption of the incident polarized light. LD intensity increases upon transformation from fibers to 2D sheets (Figure 4b) due both to increased chromophore density and higher alignment of the chromophores. In this case, the elongated nature of the **ASP-1** amphiphile results in alignment of the chromophores within the film upon compression at the water surface. Since the substrate for LB deposition is oriented parallel with the barrier, films of **ASP-1** lifted from the air–water interface have their component molecules aligned perpendicular to the direction of substrate dipping. Moreover, the molecular dipole moment (estimated to be 2.45 D using DFT calculations at the B3LYP/6-31G** level; see Figure S2b, Supporting Information) coincides approximately with the long axis of the **ASP-1** molecules so that the transition dipole moment (TDM) should be similarly oriented.[42,43] Increasing LD intensity with increasing surface pressure while peak position is maintained at the same wavelength suggests a compression-induced orientation of the dipole moments in the 2D sheets. These factors account for the large increasingly negative response of **ASP-1** in the 2D sheets where chromophores are aligned perpendicular to the sheet long axis (established by the substrate dipping direction during LB multilayer fabrication).

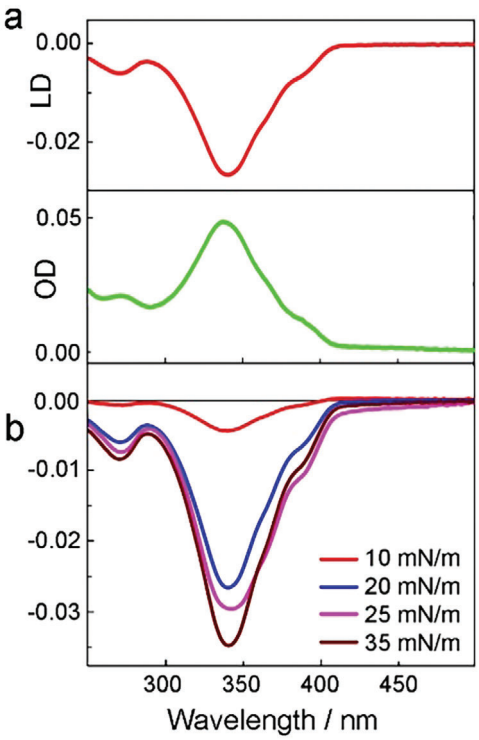

Figure 4. Linear dichroism (LD) of 59-layered **ASP-1** LB films lifted at different surface pressures. a) LD and UV–vis spectra of **ASP-1** 2D sheets of multilayered films. Significant negative LD signal indicating greater perpendicular (A⊥) than parallel (A∥) absorption of polarized light. b) Surface pressure dependency of LD. c) Compressed monolayer of **ASP-1** molecules with SP long axes parallel to compressing barriers (responsible for the negative LD response).

Having established the alignment of the molecules within the 2D sheet based on limiting molecular area (**Figure** 5a), dipping direction (Figure 5b) and LD spectroscopy (Figure 4), grazing incidence X-ray diffraction (GIXD) of a multilayer LB film was carried out using synchrotron radiation in order to further define the structure of **ASP-1** 2D sheets (Figure 5c). An alternating lamellar type structure of the film is implied based on the LB approach for multilayer films (here n = 50 layers) since hydrophilic and hydrophobic moieties will be segregated in the resulting multilayered nanostructure (Y-type film structure[44,45]). In this case,

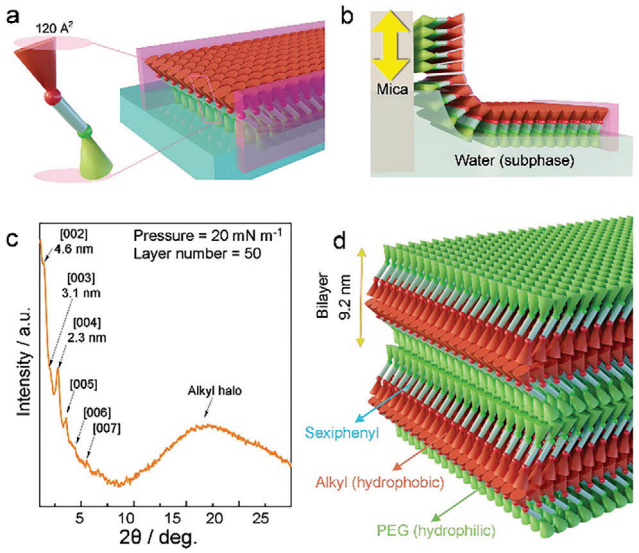

Figure 5. Structure of multilayered **ASP-1** LB films. a) Schematic illustrating the limiting molecular area ($A = 120$ Å^2) and its origin. b) Method for preparation of multi-layered film by repetitive immersion and withdrawal of a mica substrate through the compressed monolayer of **ASP-1** at the air–water interface. c) Synchrotron GIXD scattering pattern of a 50-layer LB film lifted at $\pi = 20$ mN m^{-1} Major reflections indicate a lamellar structure. The [001] reflection is obscured beyond the beamstop. d) Bilayer structure of the **ASP-1** LB film assembly established based on amphiphilic **ASP-1** in the LB method. Important regions of the 'Y'-type layered structure are indicated.

the compound has the form dendron(A)-rod-dendron(B) (by analogy with dendron-rod-coil structures[46]) where sexiphenyl is the "rod". The alternating lamellar structure of the multilayer film and its dimensions give rise to the observed GIXD reflections as shown in Figure 5c. It is a lamellar structure based on a 9.2 nm thick bilayer. A lamellar structure is also supported by transmission electron microscopy (TEM) observations (Figure S4, Supporting Information). Based on the characteristics of **ASP-1** 2D sheets, a model of the nanostructured film is shown in Figure 5d.

It is interesting to compare this lamellar phase with the structure of **ASP-1** in its bulk solid state obtained under thermotropic conditions (i.e., in the absence of an air–water interface). In that case, although a peak appears at a similar position to the monolayer films at 4.51 nm in the scattering pattern of as-isolated **ASP-1** (possibly suggesting that the material has a similar alternating lamellar structure), that pattern also presents a peak having a base dimension of 6.1 nm following cooling of a sample of **ASP-1** from an isotropic state (≈270 °C) (Figure S5, Supporting Information). That is, while some compounds are known to form thermotropic bilayer structures based on molecular amphiphilicity,[47] **ASP-1** does not. The obvious difference in structure of **ASP-1** under thermotropic conditions highlights the importance of using the air–water interface to obtain uniquely nanostructured materials. In this case, it is also important to note that the LB method is performed under ambient conditions while thermotropic processing of **ASP-1** to an isotropic state involves elevated temperatures and inevitably risks decomposition of the subject molecules.

2.5. PL Polarization in ASP-1 Films

Based on the molecular orientation of **ASP-1** within multilayered 2D sheets (Figure 5d), we performed polarization-angle-dependent photoluminescence spectroscopy. The sheet exhibits polarized PL with greatest emission intensity at ≈0° and 180°, and weakest emission at angles ≈90° and 270°. This indicates that polarization of the **ASP-1** emission at 407, 431, and 454 nm is strongly directed parallel to the 2D sheets, with a variation in intensity dependent on the polarizer angle (see **Figure 6a**).[15] Starting at 0°, emission intensity is gradually attenuated as the polarizers are rotated to a vertical position (90°) where it reaches a minimum, as shown in Figure 6b. PL intensity then gradually increases returning to the starting value by rotation of the polarizers to 180°. According to polarized PL spectra,[48] the multilayer 2D sheet of **ASP-1** molecules exhibits extremely strong anisotropy. The intensity ratio, $I_r = (I\| - I\perp)/ (I\| + I\perp)$, versus polarization angle, was used to determine the polarization ratio (I_r), which was found to be ≈0.8. (Figure 6c). This high polarization ratio indicates a well-oriented and uniformly ordered structure of the 1D **ASP-1** molecules contained in the LB films so this 2D sheet has excellent potential as a polarized luminescent material.[14,48,49] A schematic of the PL polarization measurement is shown in Figure 6d, and polarization of the 2D sheets was verified using an optical microscope equipped with cross-polarizers (Figure 6e,f). The 2D sheets appear bright under parallel polarization conditions but are dark under cross-polarization.

Large values of I_r have been reported for other materials usually associated with a highly oriented internal structure. In our previous work,[13,15,16] we have obtained similar values of polarization from materials with structures based on liquid crystal alignment of nanomaterials or self-assembled fibers (0.8 – 0.9). Other workers have also reported useful levels of PL polarization ratio as high as 0.95 in polymers,[50,51] self-assembled organic nanomaterials[52,53], and in solid state nanomaterials.[54,55] This demonstrates that **ASP-1** is competitive with state-of-the-art materials in terms of its PL polarization ratio characteristics, but it has additional benefits such as ease of preparation and flexibility of the synthesis concept. That is, it is a simple matter to vary the active element (here sexiphenyl) to obtain polarized emission in a wide variety of organic chromophores in turn allowing coupling of this property with other salient characteristics. For example, sexiphenyl **ASP-1** also exhibits semiconductivity with diode-like behavior in its 2D sheet form (see Figure S6, Supporting Information) as well as an easy first reduction at −1.3 V (see Figure S7, Supporting Information). These additional properties imply that the presented treatment of chromophores for formation of 2D sheet might be applied for incorporation of these materials in electronic devices aimed at diverse uses including sensing, switching, or data storage. Our current research is aimed at developing such multifunctional materials systems for advanced optoelectronic applications.

3. Conclusion

The amphiphilic linear sexiphenyl derivative **ASP-1** assembles during compression at air–water interface forming uniform large 2D sheets whose film packing properties improve with increasing applied surface pressure. **ASP-1** exhibits large PL quantum

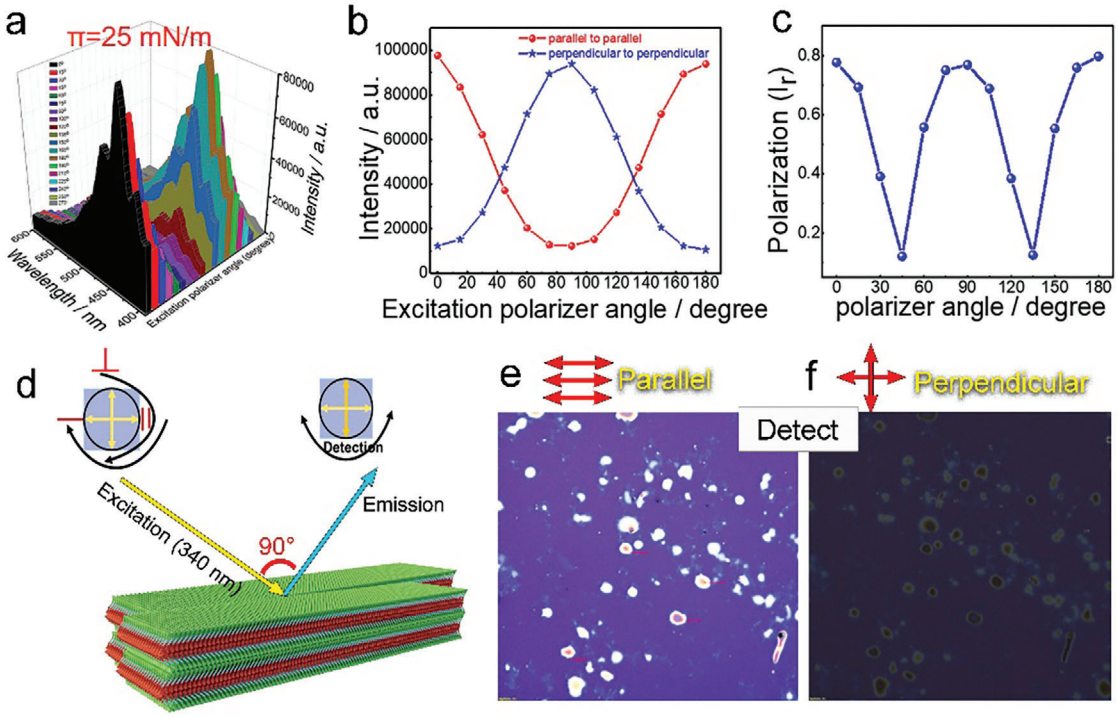

Figure 6. Film structure and polarization of photoluminescence (PL) in **ASP-1** LB multilayer films. a–c) **ASP-1** molecules are forced with long axes parallel to film but perpendicular to substrate (mica) dipping direction. Blue arrows in **c** indicate approximate molecular dipole axis. d) Film viewed from top showing relative orientation of molecular long axes (and bulk dipole) against dipping direction. e) Geometry of measurement of fluorescence polarization and representative fluorescence images. f) Dependence of the PL spectra of an **ASP-1** LB film as a function of the polarizer rotation angle in a multilayer film lifted at a surface pressure of 25 mN m^{-1}. g) Variation in PL intensity at 454 nm of **ASP-1** LB film as a function of polarizer rotation angle from 0° to 270°. h) Angle-resolved polarization (I_r) of the PL spectra.

yields in solution and when contained in multilayer film. Interestingly, multilayered films of **ASP-1** obtained using the layer-by-layer (LbL) method form a lamellar Y-type structure as demonstrated by GIXD analysis using synchrotron radiation. Orientation of the molecules in the films probed using LD spectroscopy reveals that sexiphenyl chromophores are aligned perpendicular to the film lifting direction. Based on the molecular alignment, multilayer LB film lifted at higher surface pressure exhibits strong fluorescence anisotropy with PL polarized parallel to the 2D sheet lifting direction, as indicated by polarized PL spectra. The large value of the polarization ratio clearly establishes the high degree of molecular alignment of **ASP-1** molecules within the 2D sheets obtained by using the LbL method at the air–water interface, which is a much easier-to-implement and better controllable method than substrate rubbing combined with vacuum deposition techniques used previously.[24] The ease of film preparation and its optical properties described here make **ASP-1** LB-LbL film an excellent candidate as a polarized luminescent material for applications including OLEDs, display devices, and optical information storage.

Supporting Information

Supporting Information is available from the Wiley Online Library or from the author.

Acknowledgements

This work was partly supported by World Premier International Research Center Initiative (WPI Initiative), MEXT, Japan. The authors are grateful to JST-ERATO Yamauchi Materials Space-Tectonics Project (JPMJER2003) and the Queensland Node of the Australian National Fabrication Facility (ANFF-Q). S.A. acknowledges SERB grant SERB-STAR grant #STR/2020/000053. The authors acknowledge Technical Research Centre (TRC) of IACS for experimental support. Photon Factory, KEK, Tsukuba, Japan is gratefully acknowledged for the GIXD measurements using synchrotron radiation.

[Correction added on 25th April, 2024 after online publication: Afilliations of Dr. Yusuke Yamauchi, Dr. Lok Kumar Shrestha and Dr. Somobrata Acharya was updated in this version].

Conflict of Interest

The authors declare no conflict of interest.

Data Availability Statement

The data that support the findings of this study are available in the supplementary material of this article.

Keywords

2D nanosheets, amphiphile, polarized emission, self-assembly, sexiphenyl

Received: January 20, 2024
Revised: February 23, 2024
Published online: March 14, 2024

[1] A. K. Geim, K. S. Novoselov, *Nat. Mater.* **2007**, *6*, 183.
[2] A. E. Naclerio, P. R. Kidambi, *Adv. Mater.* **2023**, *35*, 2207374.
[3] Y. Gogotsi, B. Anasori, *ACS Nano* **2019**, *13*, 8491.
[4] S. Ghosh, D. S. Philips, A. Saeki, A. Ajayaghosh, *Adv. Mater.* **2017**, *29*, 1605408.
[5] K. Ariga, Q. Ji, J. P. Hill, Y. Bando, M. Aono, *NPG Asia Mater* **2012**, *4*, e17.
[6] S. Z. Butler, S. M. Hollen, L. Cao, Y. Cui, J. A. Gupta, H. R. Gutiérrez, T. F. Heinz, S. S. Hong, J. Huang, A. F. Ismach, E. Johnston-Halperin, M. Kuno, V. V. Plashnitsa, R. D. Robinson, R. S. Ruoff, S. Salahuddin, J. Shan, L. Shi, M. G. Spencer, M. Terrones, W. Windl, J. E. Goldberger, *ACS Nano* **2013**, *7*, 2898.
[7] D. Chimene, D. L. Alge, A. K. Gaharwar, *Adv. Mater.* **2015**, *27*, 7261.
[8] T. Xiao, J. Qin, C. Peng, R. Guo, X. Lu, X. Shi, *Langmuir* **2020**, *36*, 3096.
[9] G. R. Suman, M. Pandey, A. S. J. Chakravarthy, *Mater. Chem. Front.* **2021**, *5*, 1541.
[10] A. Mukherjee, T. Sakurai, S. Seki, S. Ghosh, *Langmuir* **2020**, *36*, 13096.
[11] J. B. Birks, *Photophysics of Aromatic Molecules*, Wiley-Interscience, Hoboken, New Jersey, **1970**.
[12] R. Li, L. Jiang, Q. Meng, J. Gao, H. Li, Q. Tang, M. He, W. Hu, Y. Liu, D. Zhu, *Adv. Mater.* **2009**, *21*, 4492.
[13] S. Acharya, S. Kundu, J. P. Hill, G. J. Richards, K. Ariga, *Adv. Mater.* **2009**, *21*, 989.
[14] X. Yang, L. F. Ma, D. Yan, *Chem. Sci.* **2019**, *10*, 4567.
[15] K. Sakakibara, P. Chithra, B. Das, T. Mori, M. Akada, J. Labuta, T. Tsuruoka, S. Maji, S. Furumi, L. K. Shrestha, J. P. Hill, S. Acharya, K. Ariga, A. Ajayaghosh, *J. Am. Chem. Soc.* **2014**, *136*, 8548.
[16] S. Acharya, D. D. Sarma, Y. Golan, S. Sengupta, K. Ariga, *J. Am. Chem. Soc.* **2009**, *131*, 11282.
[17] S. S. Babu, V. K. Praveen, A. Ajayaghosh, *Chem. Rev.* **2014**, *114*, 1973.
[18] T. Nozaki, M. Tamura, Y. Harada, K. Saito, *Bull. Chem. Soc. Jpn.* **1960**, *33*, 1329.
[19] K. J. Liu, G. Hernandez-Sosa, H. Sitter, C. F. Zhang, Z. W. Dong, Y. L. Yan, S. X. Qian, *Chem. Phys. Lett.* **2007**, *446*, 83.
[20] J. Stampfl, S. Tasch, G. Leising, U. Scherf, *Synth. Met.* **1995**, *71*, 2125.
[21] W. Graupner, F. Meghdadi, G. Leising, G. Lanzani, *Phys Rev B Condens Matter Mater Phys* **1997**, *56*, 10128.
[22] D. J. Gundlach, Y. Y. Lin, T. N. Jackson, D. G. Schlom, *Appl. Phys. Lett.* **1997**, *71*, 3853.
[23] R. Resel, *Thin Solid Films* **2003**, *433*, 1.
[24] M. Era, T. Tsutsui, S. Saito, *Appl. Phys. Lett.* **1995**, *67*, 2436.
[25] J. Novák, M. Oehzelt, S. Berkebile, M. Koini, T. Ules, G. Koller, T. Haber, R. Resel, M. G. Ramsey, *Phys. Chem. Chem. Phys.* **2011**, *13*, 14675.
[26] H. Yanagi, S. Okamoto, *Appl. Phys. Lett.* **1997**, *71*, 2563.
[27] S. Maji, P. Alam, G. S. Kumar, S. Biswas, P. K. Sarkar, B. Das, I. Rehman, B. B. Das, N. R. Jana, I. R. Laskar, *Small* **2017**, *13*, 1603780.
[28] J. Mei, N. L. C. C. Leung, R. T. K. K. Kwok, J. W. Y. Y. Lam, B. Z. Tang, *Chem. Rev.* **2015**, *115*, 11718.
[29] P. Mondal, G. Manna, T. Kamilya, M. Das, K. Ariga, G. J. Richards, J. P. Hill, S. Acharya, *Adv. Mater. Interfaces* **2022**, *9*, 2200209.
[30] P. Mondal, S. Biswas, D. Jana, B. Das, U. K. Ghorai, B. K. Ghorai, S. Acharya, *J. Solid State Chem.* **2020**, *282*, 121122.
[31] D. Shi, D.-V. Nguyen, M. Maaloum, J.-L. Gallani, D. Felder-Flesch, M. P. Krafft, *Molecules* **2019**, *24*, 4114.
[32] K. N. Baker, A. V. Fratini, T. Resch, H. C. Knachel, W. W. Adams, E. P. Socci, B. L. Farmer, *Polymer* **1993**, *34*, 1571.
[33] M. Arkas, M. Douloudi, M. Vardavoulias, T. Katsika, *Symmetry* **2022**, *14*, 394.
[34] Y. Luo, C. P. Collier, J. O. Jeppesen, K. A. Nielsen, E. DeIonno, G. Ho, J. Perkins, H. Tseng, T. Yamamoto, J. F. Stoddart, *ChemPhysChem* **2002**, *3*, 519.
[35] S. Maji, A. Das, P. K. Sarkar, A. Metya, S. Ghosh, S. Acharya, *RSC Adv.* **2014**, *4*, 44650.
[36] S. Santos, V. Barcons, H. K. Christenson, J. Font, N. H. Thomson, *PLoS One* **2011**, *6*, e23821.
[37] J. Hu, D. F. Ogletree, M. Salmeron, *Surf. Sci.* **1995**, *344*, 221.
[38] S. Bhagat, W. D. Leal, M. B. Majewski, J. Simbrunner, S. Hofer, R. Resel, I. Salzmann, *Electron. Struct.* **2021**, *3*, 034004.
[39] S. Biswas, D. Jana, G. S. Kumar, S. Maji, P. Kundu, U. K. Ghorai, R. P. Giri, B. Das, N. Chattopadhyay, B. K. Ghorai, S. Acharya, *ACS Appl. Mater. Interfaces* **2018**, *10*, 17409.
[40] H. K. Bisoyi, Q. Li, *Chem. Rev.* **2021**, *122*, 4887.
[41] J. P. Hill, L. K. Shrestha, S. Ishihara, Q. Ji, K. Ariga, *Molecules* **2014**, *19*, 8589.
[42] J. G. Carter, R. Pfukwa, L. Riley, J. H. R. Tucker, A. Rodger, T. R. Dafforn, B. Klumperman, *ACS Omega* **2021**, *6*, 33231.
[43] O. A. Bell, G. Wu, J. S. Haataja, F. Brömmel, N. Fey, A. M. Seddon, R. L. Harniman, R. M. Richardson, O. Ikkala, X. Zhang, C. F. J. Faul, *J. Am. Chem. Soc.* **2015**, *137*, 14288.
[44] R. S. Singh, *Soft Mater.* **2022**, *20*, 57.
[45] A. Fujimori, in *Encyclopedia of Polymeric Nanomaterials* (Eds: S. Kobayashi, K. Muellen), Springer Berlin, Heidelberg, Germany **2015**, pp. 1044–1050.
[46] S. Lecommandoux, H. Klok, M. Sayar, S. I. Stupp, *J. Polym. Sci., Part A: Polym. Chem.* **2003**, *41*, 3501.
[47] P. H. J. Kouwer, G. H. Mehl, *J. Mater. Chem.* **2009**, *19*, 1564.
[48] A. Andreev, G. Matt, C. J. Brabec, H. Sitter, D. Badt, H. Seyringer, N. S. Sariciftci, *Adv. Mater.* **2000**, *12*, 629.
[49] X. G. Yang, J. H. Qin, Y. D. Huang, Z. M. Zhai, L. F. Ma, D. Yan, *J. Mater. Chem. C* **2020**, *8*, 17169.
[50] S. V. Ulrich, T. Sutch, G. Szulczewski, M. Schweizer, N. W. Barbosa Neto, P. T. Araujo, *J. Phys.: Condens. Matter* **2018**, *30*, 265101.
[51] W. Gong, G. Huang, M. Zhou, C. Fan, Y. Yuan, H. Zhang, *ACS Appl. Mater. Interfaces* **2023**, *15*, 49701.
[52] Y. Che, X. Yang, K. Balakrishnan, J. Zuo, L. Zang, *Chem. Mater.* **2009**, *21*, 2930.
[53] D. Yan, H. Yang, Q. Meng, H. Lin, M. Wei, *Adv. Funct. Mater.* **2014**, *24*, 587.
[54] M. Hasegawa, Y. Hirayama, S. Dertinger, *Appl. Phys. Lett.* **2015**, *106*, 051103.
[55] H.-Y. Chen, Y. C. Yang, H.-W. Lin, S.-C. Chang, S. Gwo, *Opt. Express* **2008**, *16*, 13465.